Pharmaceutical Nickel(II) Chelation Properties of 3-Hydroxyflaven, Deferiprone and Maltol Metal Chelators: A Density Functional Study

S. Salehi[a,b,*], S.M. Mashmool Moghaddam[a], M. Tarin[a] and A. Shokooh Saljooghi[a,*]

aDepartment of Chemistry, Faculty of Sciences, Ferdowsi University of Mashhad, Mashhad, Iran
bFaculty of Chemistry, University of Mazandaran, Babolsar, Iran
(Received 19 September 2019, Accepted 29 November 2019)

The present study describes the metal chelating ability of 3-hydroxyflavene, deferiprone and maltol with Ni^{2+} metal ion using density functional theory. Structural analysis indicates that all three chelators bind to Ni^{2+} ion as a two-dentate chelator. Donor-acceptor interactions show an effective charge transfer from the oxygen atoms of the chelators towards Ni^{2+}. Quantum theory of atoms in molecules analysis shows that the non-covalent interactions, mainly, electrostatic interactions play an important role in the complex formation of the selected chelators and Ni^{2+} ion. The TD-DFT study was applied in order to investigate the main electron transition. The ELF and LOL analyses were applied to confirm the results obtained from the QTAIM analysis. Interaction energies and metal ion affinity were calculated for the $[Ni(L)_2]$ complexes and the results revealed a highly exothermic reaction during the chelation process. The natural bond analysis (NBO), natural population analysis (NPA) and spin density evaluation were carried out to evaluate the charge transfer in the complexes. The NCI-RDG isosurface of the studied complexes show a complete set of electrostatic interactions including Van der Waals interactions. On the basis of the results, the selected chelators could be considered as the effective chelating agents for Ni therapy.

Keywords: Metal chelators, Toxic metals, Nickel, DFT, QTAIM

INTRODUCTION

The effect of excess metal ions in numerous vital biological mechanism, which is reflected in metalloproteins composed of approximately one third of the proteome, has been the subject of many studies [1]. Rapid development of modern industrial and agricultural activities led to increase in the level of different heavy metals' concentrations in the environmental stress which are considered as the most important factor of numerous metal ion-associated diseases [2]. Nowadays, the exposure of heavy metals such as Fe, Zn, Cd, Ni and Pb in the environment are the greatest threat to public health [3]. It is proven that diseases such as Wilson disease, diabetes mellitus, Alzheimer disease and β-thalassemia are directly associated with the level of metal ions [4-5].

Nickel is a metal commonly used to make coins, magnets, jewelry, stainless steel, electronics and components of industrial machines [6]. It is beleived that the toxicity of nickel arises from the essential metal imbalancement in biological systems [7]. It also severely disrupts enzyme's function and regulation, and contributes to a high level of oxidative stress [8]. The effect of chronic exposure of nickel in development of diseases such as lung cancer, cardiovascular disease, neurological deficits [9], and developmental deficits in childhood [8], and high blood pressure have been subject of different studies [10].

Detoxification of metal species in biological inhabitants is performed through different procedures of chelation such as synthetic, chemical and peptide chelators [11]. Among them organic molecules named as metal chelating agents consist of inherent functionality able to capture and bind specific metal ions are much of interest. Many studies have employed coordination chemistry in designing effective

─────────────
*Corresponding authors. E-mail: samiesalehi@gmail.com; saljooghi@um.ac.ir

chelators for toxic metal chelation [12,13].

Nowadays, there are several kinds of chelating agents used extensively for the clinical treatment of the transfusion induced metal ions overload [14]. However, the efforts to find suitable metal chelators which are capable to chelate to other metal cations involved in the human disease are under development.

In the present study, three classes of organic molecules named 3-hydroxyflavene (HL$_f$) [15], deferiprone (3-hydroxy-1,2-dimethylpyridin-4-one) (HL$_d$) [16] and maltol (2-methyl-3-hydroxy-4H-pyran-4-one) (HL$_m$) [17] were considered to investigate their pharmaceutical chelation properties of nickel ion. However, their chelation properties in detoxification of different metal ions have been investigated experimentally. It is assumed that all three molecules are chelated with the metal centers through their carbonyl and hydroxyl groups [18]. The efficiency of HL$_f$ in chelation with metal ions such as Al^{3+}, Fe^{2+}, Fe^{3+}, Cu^{2+}, or Zn^{2+} was reported previously [19]. HL$_d$ has also been reported to be able to cross the brain-blood barrier due to its small molecular weight and currently is considered as one of the main candidates for development of orally active iron chelators [20]. Some studies confirmed the HL$_m$ ability in chelation with metal ions such as gallium, as well as with iron, zinc, aluminum and vanadium [22]. The chemical structure of three metal chelators are represented in Fig. 1.

Despite of many studies which are associated with measuring the level of metal ions by using the experimental methods, understanding the chelating property of metal chelators including their electronic and geometrical properties in a theoretical methods can complement experimental studies [23,24]. Nowadays, different theoretical methods, mainly quantum mechanical (QM) and molecular dynamic (MD) methods, have been developed to predict different biological processes either in the presence or absence of toxic metal ions in a theoretical view [25-26]. These methods provide a deep insight of these processes which would clarify the complicated biological process [27]. In our previous studies, computational methods were employed to investigate the stability of iron chelators in iron uptake process [28]. In the present study, we have investigated the chelating properties and metal ion selectivity of 3-hydroxyflavene (HL$_f$), deferiprone (HL$_d$) and maltol (HL$_m$) in chelation of Ni^{2+} metal ion using

density functional theory (DFT). We have also studied the chelation property of the metal complexes mentioned in both gas and solvent (water and DMSO) phases. This study will clarify the structural properties of [Ni(L)$_2$] complexes and may be helpful in selecting the appropriate chelating agent.

Computational Details

Geometry optimization were performed at the M062x/6-311++G(d,p) level of theory using the Gaussian09 computational package [29]. Frequency calculations to estimate the zero-point vibrational energies (ZPVEs), for all structures in the gas phase and solvents, and to confirm the stability of the structures with the real frequencies were performed. Stability and equilibrium constants of complexes were calculated at 298.15 K according to the experimental conditions. The solvents (water and DMSO) effects on the binding process of metal chelators to Ni(II) ion were investigated. To do so, the conductor like polarizable continuum model (CPCM) was applied [30]. Natural bond orbital analysis (NBO) analysis in the M062x/6-311++G (d,p) level was carried out to explore the distribution of electrons into the atomic and molecular orbitals and contributions of covalent interactions to the high chemical specificity of the [Ni(L)$_2$]$^{2+}$ (L$_f$: 3-hydroxyflavone, L$_d$: deferepirone and L$_m$: maltol) complexes [31]. Quantum chemistry reactivity indices of the isolated compounds were determined in order to describe the reactivity trend in complexes. Topological properties were analyzed using the Bader's theory of atoms in molecules in AIM2000 package using the wave functions generated from the M062x/6-311++G(d,p) results [32]. Furthermore, to investigate the nature of interactions between Ni(II) ion and selected metal chelators, the electron localization function (ELF), localized orbital locator (LOL), two-dimensional (2D) and three-dimensional (3D) noncovalent interaction (NCI) plots were carried out using Multi-WFN 3.4 [33]. The spin density of chelated complexes was also calculated in the same method to investigate the influence of chelation process on spin density distribution on Ni^{2+}. Additionally, TD-DFT method was applied to investigate the electronic transition properties of complexes [34]. The minimum molecular electrostatic potential (MESP) was investigated as well. The optimized structures were used to evaluate the interaction
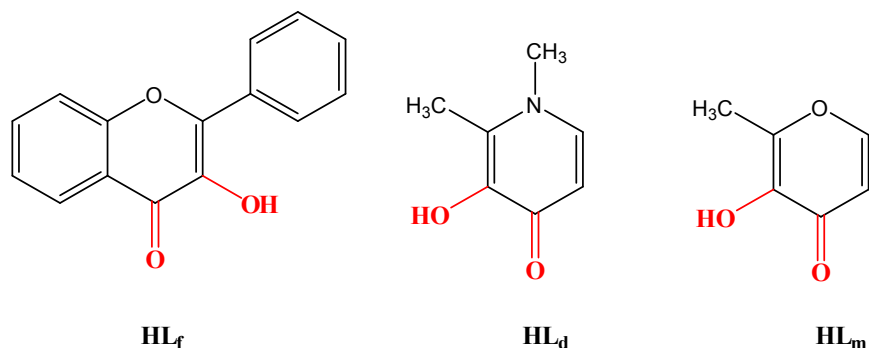
Fig. 1. The chemical structures of HL_f, HL_d and HL_m metal chelators.

energy values of the HL_f, HL_d and HL_m complexes with Ni^{2+} metal ion. The Ni-L interaction energies of these complexes have been calculated according to Eq. (1):

$$\Delta E_{interaction} = E_{complex} - E_M - E_{HL} \qquad (1)$$

where $E_{complex}$ represents the total energy of the $[Ni(L)_2]$ complexes and E_M and E_{HL} are the total energies of Ni^{2+} and isolated chelators (HL_f, HL_d and HL_m), respectively. In order to study the stability of the metal-ligand interactions the metal ion affinity (MIA) and the corresponding values were computed for the $[Ni(L)_2]$ chelation process as shown in Eq. (2) [35].:

$$MIA = -[E_{el}(complex) - E_{el}(HL) - Eel(Ni^{2+}) + (E_{vib}(complex) - E_{vib}(HL) \qquad (2)$$

where E_{el} is the electronic energy obtained through the SCF computation and E_{vib} includes the zero-point energy. The temperature corrections from 0 to 298 K [36,37] were obtained by the thermochemical analysis of vibrational frequencies.

Local Bonding Structure and Equilibrium Constant

The geometry of the 1:2 $[Ni(L)_2]$ complexes are obtained by the interaction of [Ar] $3d^8$ orbitals of Ni^{2+} metal ion and chelators' orbitals. The optimized structural parameters of $[Ni(L)_2]$ complexes at gas and solvent phases are shown in Tables S1 and S2, respectively. The Ni^{2+} metal ion is coordinated to the oxygen atoms of HL_f, HL_d and

HL_m metal chelators. The coordination distances of O1(28)-Ni^{2+}, O2(29)-Ni^{2+} interactions are found to be 1.922 and 2.053 Å for $[Ni(L_f)_2]$ complex. The O1(19)-Ni^{2+}, O2(20)-Ni^{2+} distances are 1.895 and 1.912 Å for $[Ni(L_d)_2]$ complex, and O1(14)-Ni^{2+}, O2(15)-Ni^{2+} distances are 1.881 and 1.886Å for $[Ni(L_m)_2]$ complex in the gas phase. From the results obtained for the $[Ni(L_m)_2]$ complex, it is inferred that the L_m-Ni^{2+} complex shows the shorter coordination distance than that for the L_d-Ni^{2+} and L_f-Ni^{2+} complexes.

The C4-O1 and C5-O2 bond lengths of parent 3-hydroxyflaven (L_f) are found to be 1.249 and 1.218 Å calculated at same levels of theory, respectively. Since there is a profound charge transfer from the oxygen atoms of L_f to the metal ion, the bond lengths of C4(31)-O1(28) and C5(32)-O2(29) are found to be elongated by 0.09 Å for $[Ni(L_f)_2]$ complex. The bond lengths calculated for C5-O1 and C6- O2 in L_d are 1.283 and 1.258 Å, and for C4-O1 and C5-O2 in L_m are 1.258 and 1.227Å for the free ligands, while, due to charge transfer into the Ni^{2+} ion, the C5(21)-O1(19) and C6(22)-O2(20) bond lengths in L_d are elongated by 0.02 and 0.05Å for $[Ni(L_d)_2]$ and the C4(16)-O1(14) and C5(17)-O2(15) bonds are found to be elongated by 0.04 and 0.06Å for $[Ni(L_m)_2]$.

The coordination distances of L_f-Ni^{2+} complex in water and DMSO as solvent are found to be elongated by 0.03 Å for O1(28)-Ni^{2+}, and 0.003Å for O2(29)-Ni^{2+}coordination bonds. Similarly, the coordination distances of L_d-Ni^{2+} complex is found to be elongated by 0.09 and 0.05Å for O1(19)-Ni^{2+} and O2(20)-Ni^{2+} coordination bonds in the water and 0.06 and 0.07 Å in DMSO, respectively. Also, the

same trends were observed for L_m-Ni^{2+} bond length which the O1(14)-Ni^{2+}, O2(15)-Ni^{2+} bond lengths increased by 0.06 and 0.07 Å in the water and 0.07 and 0.08 Å in DMSO, respectively.

The thermodynamic parameters of the metal-chelator complexes were calculated using the procedure described in previous studies [20,21]. Considering the stoichiometry of the complex, 1:2, the reaction can be represented in a simple form as:

$$M^{2+} + 2L \rightarrow C$$
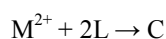
where M: Ni (II) ion, L: chelator (L_f: 3-hydroxyflavone, L_d: deferepirone and L_m: maltol), and C: metal complex [Ni(L)$_2$].

Thermodynamic parameters of all complexes such as absolute values of the Gibbs energy, entropy, enthalpy and the stability constant of the studied complexes are provided in Table 1. According to the results depicted in Table 1, the solvent has a different effect on the thermodynamic of [Ni(L)$_2$]. In the L_f-Ni complex, the stability of complexes in the DMSO is more than that in the water and gas, while the most stable complexes for L_d-Ni and L_m-Ni are observed in the water and gas, respectively. The stability of the L-Ni complexes is according to [Ni(L$_d$)$_2$] > [Ni(L$_m$)$_2$] > [Ni(L$_f$)$_2$] both in the gas and solvent.

The metrical parameter τ_4 is a useful parameter in the geometry determination of four coordinate complexes [38]. The coordination geometry of the tetra dentate coordination mode of [Ni(L)$_2$] complexes were determined using Eq. (3):

$$\tau 4 = \frac{360° - (\alpha + \beta)}{141°} \tag{3}$$

where α and β are the two largest θ angles in the four coordination complexes. According to the above equation, the value of τ_4 will range from 1.00 for a perfect tetrahedral and zero for perfect square planar geometries [38]. Based on the Eq. (1), the value of τ_4 is found to be in the range of 0.58 for the [Ni(L$_f$)$_2$] complex in the both gas and solvent phases, 0.61-0.59 for the [Ni(L$_d$)$_2$] and [Ni(L$_m$)$_2$] complexes in the gas and solvents phases, respectively, which are found to prefer the distorted tetrahedral coordination geometry.

Electron Localization Function and Localized Orbital Locator

Figure 2 and Table 2 show the LOL and ELF diagrams of the interaction between the metal center and chelators studied in the gas phase. Generally, large and small values of the LOL and ELF parameters indicate the covalent and electrostatic interactions, respectively [39]. According to Fig. 2, LOL and ELF values are small, confirming an electrostatic interaction between the metal chelators and the Ni(II) ion. Moreover, Table 2 lists the Ni-O bonds, ELF and LOL values in the gas, water and DMSO.

Interaction Energies and MIA

To gain a deep insight into the stability of the interaction of [Ni(L)$_2$] chelated complexes, the interaction energies have been calculated at M062x/6-311++G(d,p) levels of theory and the obtained results for gas, water and DMSO are reported in Table 3. It could be concluded, that the chelation process is highly exothermic due to the negative interaction energy values for all complexes confirming the results represented in Table 1. The interaction energies of [Ni(L)$_2$] complexes in the gas phase areas follows [Ni(L$_f$)$_2$] > [Ni(L$_m$)$_2$] > [Ni(L$_d$)$_2$] with the values -809.79, 476.92 and -457.32 kcal mol^{-1}, respectively.

The MIA value of metal complexes, indicating the stabilization of complexes, are found to be 672.81, 383.28 and 391.34 for the [Ni(L$_f$)$_2$], [Ni(L$_d$)$_2$] and [Ni(L$_m$)$_2$] complexes, respectively. Similar to the IE, it is observed that the destabilization of chelated complexes is follows as [Ni(L$_f$)$_2$] > [Ni(L$_m$)$_2$] > [Ni(L$_d$)$_2$]. The [Ni(L$_d$)$_2$] complex is more destabilized rather than two other complexes which could be attributed to a lower IE for these complexes. Moreover, the more IE value is, the more stabilization is observed for the complexes.

Furthermore, the inclusion of solvent effect to [Ni(L)$_2$] induces the significant variations in both the interaction energy and MIA values. It is worthy to note that the stability of the [Ni(L$_f$)$_2$] complexes in the solvent phases are found to be reduced by 0.78 kcal mol^{-1}. This value for [Ni(L$_d$)$_2$] was calculated as 3.42 and 1.33 kcal mol^{-1} in the water and DMSO, respectively. The stabilizing amounts for [Ni(L$_m$)$_2$] in the water and DMSO solvents are 0.96 and 1.97 kcal mol^{-1}, respectively. It was also found that the [Ni(L$_f$)$_2$] complex has the highest binding affinity towards

Table 1. Thermodynamic Properties and Optimized Structures of Chelators and their Corresponding [Ni(L)$_2$] Complexes in the Gas, [Water] and {DMSO} Solvents

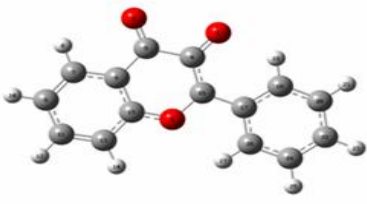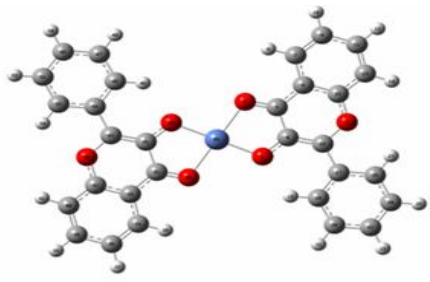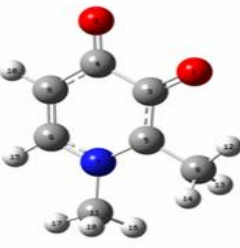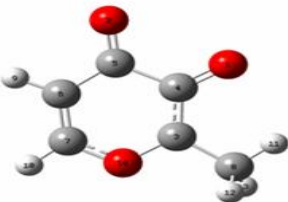|	ΔG (kcal mol^{-1})	ΔH (kcal mol^{-1})	ΔS (cal mol K^{-1})	logk
[Ni(L$_f$)$_2$]	**L$_f$**		**[Ni(L$_f$)$_2$]$^{2+}$**	
	-182.0	-200.8	-72.0	70.5
	[-100.4]	[-106.7]	[-69.0]	[73.6]
	{-106.7}	{-100.4}	{-63.4}	{78.1}
[Ni(L$_d$)$_2$]	**L$_d$**		**[Ni(L$_d$)$_2$]$^{2+}$**	
	-119.2	-119.2	-82.8	87.3
	[-238.5]	[-232.2]	[-80.7]	[174.8]
	{-213.4}	{-219.6}	{-81.2}	{156.4}
[Ni(L$_m$)$_2$]	**L$_m$**		**[Ni(L$_m$)$_2$]$^{2+}$**	
	-106.7	-131.8	-79.1	78.2
	[-115.2]	[-126.5]	[-64.1]	[83.8]
	{-138.1}	{-119.2}	{-66.6}	{101.2}

Table 2. Calculated Values for the ELF and LOL at BCPs of the Ni-O Bonds in [Ni(L)$_2$] Complexes. Values within the Parentheses and Brackets Represent the Results Obtained at Water and DMSO Solvent Phase, Respectively

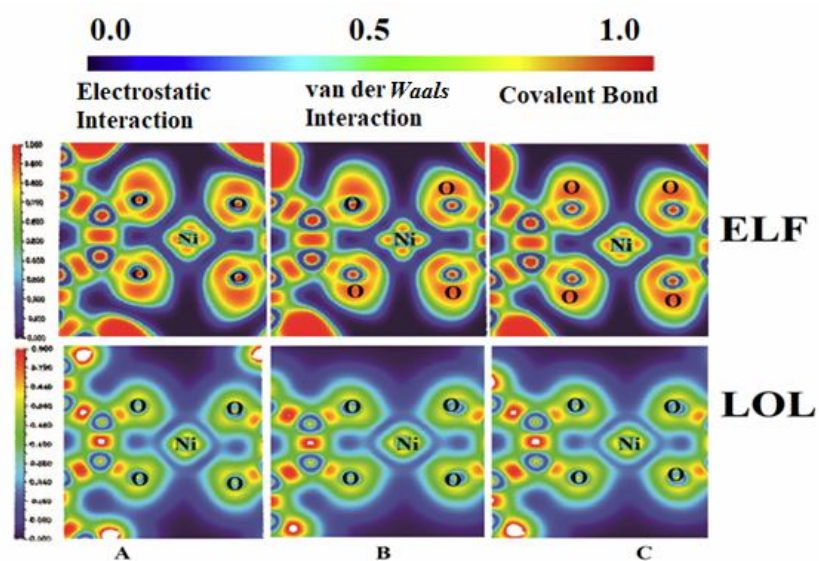| Complex	Bond	ELF	LOL
[Ni(L$_f$)$_2$]	Ni-O1(28)	0.128	0.275
		(0.123)	(0.271)
		[0.123]	[0.271]
	Ni-O2(29)	0.091	0.236
		(0.089)	(0.233)
		[0.089]	[0.233]
[Ni(L$_d$)$_2$]	Ni-O1(19)	0.107	0.256
		(0.123)	(0.271)
		[0.122]	[0.269]
	Ni-O2(20)	0.101	0.252
		(0.102)	(0.248)
		[0.094]	[0.239]
[Ni(L$_m$)$_2$]	Ni-O1(14)	0.131	0.277
		(0.100)	(0.245)
		[0.124]	[0.271]
	Ni-O2(15)	0.107	0.254
		(0.116)	(0.264)
		[0.089]	[0.233]

Fig. 2. Gas phase ELF and LOL plots of A) [Ni(L$_f$)$_2$], B) [Ni(L$_d$)$_2$] and C) [Ni(L$_m$)$_2$].

Table 3. Interaction Energies (in kcal mol^{-1}) for the [Ni(L)$_2$] Metal Complexes, Calculated at M062x/6-311++G(d,p) Levels of Theory for Gas, Water and DMSO Solvent Phases. Values within the Parentheses and Brackets Represent the Results Obtained at Water and DMSO Solvent Phases, Respectively

[Ni(L$_f$)$_2$]		[Ni(L$_d$)$_2$]		[Ni(L$_m$)$_2$]	
IE	MIA	IE	MIA	IE	MIA
-802.79	672.81	-476.92	383.28	-457.32	391.34
(-803.72)	(673.59)	(-472.74)	(386.70)	(-457.29)	(392.20)
[-803.72]	[673.59]	[-472.85]	[384.61]	[-457.39]	[393.31]
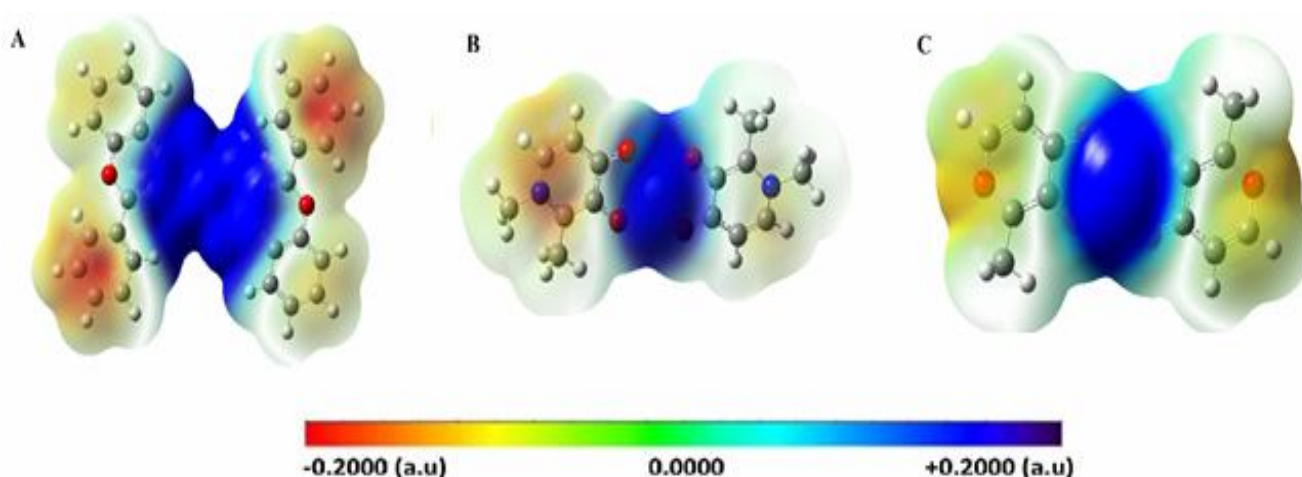
Fig. 3. MESP isosurfaces for A) [Ni(L$_f$)$_2$], B) [Ni(L$_d$)$_2$] and C) [Ni(L$_m$)$_2$].

HL$_f$ in both gas and solvent phases, confirmed by their higher interaction energy values. At the gas phase, the interaction energies and MIA values of the complexes calculated in this study follow the order [Ni(L$_f$)$_2$] > [Ni(L$_d$)$_2$] > [Ni(L$_m$)$_2$] and [Ni(L$_f$)$_2$] > [Ni(L$_m$)$_2$] > [Ni(L$_d$)$_2$], respectively.

Electrostatic potential (ESP) map is considered as one of the useful methods to evaluate and predict the reactive sites of a molecule in biological systems [40]. Different values of the ESP on the surface are represented by different colors, according to: red < orange < yellow < green < blue. The blue regions show electron deficiency (nucleophilic reactivity), and the red regions show relative abundance of electron (electrophilic reactivity). Figure 3 depicts the

MESP isosurfaces for [Ni(L$_f$)$_2$], [Ni(L$_d$)$_2$] and [Ni(L$_m$)$_2$] in the gas, water and DMSO solvents. Based on Fig. 3, oxygen atoms are the reactive nucleophilic centers for coordination with Ni^{2+}. This observation is compatible with the NBO analysis of these complexes.

TD-DFT Study

The electronic spectra of the [Ni(L)$_2$] complexes were calculated by the TD-DFT method at the m062x/6-311++g(d,p) level of theory. The TD-DFT principal electronic transitions, excitation energies and oscillator strengths are summarized in Table 4, together with the major one-electron transitions contributing to the excited-state of complexes.

Table 4. Simulated Wavelengths (nm), Energies (eV), Oscillator Strengths, and Major Contributions for $[Ni(L)_2]$ Complexes. Values within the Parentheses and Brackets Represent the Results Obtained at Water and DMSO Solvent Phases, Respectively

Complex	Wavelength (nm)	Energy (cm^{-1})	Oscillator strength	Excitation (%composition)
$[Ni(L_f)_2]$	354	28237.5	0.96	H-1(A)- > L+1(A) (15%), HOMO(A)- > LUMO(A) (32%)
	[361]	[27692.2]	[1.15]	[H-1(A)- > L+1(A) (17%), HOMO(A)- > LUMO(A) (30%)]
	{362}	{27561.6}	{1.19}	{H-1(A)- > L+1(A) (17%), HOMO(A)- > LUMO(A) (30%)}
$[Ni(L_d)_2]$	286	34901.2	0.38	H-1- > L+3 (24%), HOMO- > L+2 (65%)
	[346]	[28867.4]	[0.20]	[HOMO(A)- > LUMO(A) (45%)]
	{272}	{36708.7}	{0.16}	{H-1(A)- > L+2(A) (11%), HOMO(A)- > L+1(A) (16%)}
$[Ni(L_m)_2]$	301	33177.6	0.33	H-1(A)- > L+1(A) (13%), HOMO(A)- > LUMO(A) (35%)
	[343]	[29077.1]	[0.20]	[HOMO(A)- > LUMO(A) (47%)]
	{281}	{35492.43}	{0.38}	{H-1(A)- > L+1(A) (14%), HOMO(A)- > LUMO(A) (26%)}

Table 5. Calculated Second-order Perturbation Energies of the Donor-acceptor Interactions (kcal mol^{-1}) for $[Ni(L)_2]$ Complexes at the M062x/6-311++G(d,p) Level of Theory. Values within the Parentheses and Brackets Represent the Results Obtained at Water and DMSO Solvent Phases, Respectively

$[Ni(L_f)_2]$		$[Ni(L_d)_2]$		$[Ni(L_m)_2]$	
Donor-acceptor	$\Sigma E2$	Donor-acceptor	$\Sigma E2$	Donor-acceptor	$\Sigma E2$
$LP_{O1} \rightarrow LP^*_{Ni}$	125.9 (66.5) [84.5]	$LP_{O1} \rightarrow LP^*_{Ni}$	161.7 (48.1) [52.2]	$LP_{O1} \rightarrow LP^*_{Ni}$	64.3 (46.3) [53.2]
$LP_{O2} \rightarrow LP^*_{Ni}$	84.9 (75.2) [70.7]	$LP_{O2} \rightarrow LP^*_{Ni}$	153.8 (50.7) [41.5]	$LP_{O2} \rightarrow LP^*_{Ni}$	60.2 (49.4) [37.3]
$LP_{O28} \rightarrow LP^*_{Ni}$	121.0 (110.0) [85.3]	$LP_{O19} \rightarrow LP^*_{Ni}$	168.4 (54.0) [46.5]	$LP_{O14} \rightarrow LP^*_{Ni}$	64.2 (54.1) [53.3]
$LP_{O29} \rightarrow LP^*_{Ni}$	91.4 (79.2) [58.3]	$LP_{O20} \rightarrow LP^*_{Ni}$	151.8 (52.0) [41.6]	$LP_{O15} \rightarrow LP^*_{Ni}$	60.3 (47.3) [37.1]

A peak observed at 354 nm for $[Ni(L_f)_2]$ complex in the gas phase is assigned to the more contribution of the H→L excitation and less contribution of H-1→L+1 excitations. Clearly, the solvent caused a red shift in this complex to 361 and 362 nm in water and DMSO, respectively. However, the main orbital contribution is the same as gas phase. With the change of chelator type into L_d, a peak is appeared at 286 nm which is assigned to the more contribution of H→L+2 and less contribution of H-1→L+3 excitation. Moreover, the solvent has different effects on the transition of the $[Ni(L_d)_2]$ complex; a red shift to 346 nm is observed in water due to H→L orbitals while a blue shift to 272 nm is observed in DMSO due to H→L+1(16%) and H-1→L+2 (11%). The same results were obtained for the $[Ni(L_m)_2]$ complex. The 301 nm peak in the gas phase arising from more contribution of H→L and less contribution of H-1→L+1 undergoes a red shift to 343 nm and a blue shift to 281 nm in water and DMSO, respectively. The wavelength values in all three complexes could be written as $[Ni(L_f)_2] > [Ni(L_m)_2] > [Ni(L_d)_2]$ in the gas phase which arise from the type of orbitals contributed in the excitation. For the $[Ni(L_f)_2]$ and $[Ni(L_m)_2]$ cases, the more orbital contribution in the transition is due to H→L orbitals while this transition in $[Ni(L_d)_2]$ is due to H→L+2 which has more energy and consequently lower wavelength.

NBO Analysis

Second-order perturbation energy (E2) for delocalization of electron density between the occupied Lewis type (bonds or lone pairs) NBO orbitals and formally unoccupied (antibonds and Rydbergs) non Lewis NBO orbitals could be a good criterion for justification of the bond electron density [41]. Donor-acceptor interactions for $[Ni(L_2)]$ complexes are between LP_O and LP^*_{Ni} orbitals. As known in the NBO analysis, the greater value of the stabilization energy, E(2), represents more efficient natural charge transfer interaction between donor-acceptor species [42]. According to Table 5, the strength of donor atoms interaction with antibonding orbital of Ni atom (LP^*_{Ni}) in $[Ni(L_f)_2]$ complex in gas phase shows the $LP_{O1} > LP_{O28} > LP_{O29} > LP_{O2}$ trend, however, a different trend was observed in the presence of solvents. The strength of donor interactions to the LP^*_{Ni} changed to $LP_{O28} > LP_{O29} > LPO2 > LPO1$ and $LPO28 > LPO1 > LPO2 > LPO29$ in the water

and DMSO, respectively. Clearly, solvent reduced the electron transferring from LPO→LP*Ni which could interpret the equilibrium constant values in table. The less electron donating to the antibonding orbitals, the more equilibrium constant value.

The gas phase electron donation of O atoms to LP^*_{Ni} in $[Ni(L_d)_2]$ complex fallows as $LP_{O19} > LP_{O1} > LP_{O2} > LP_{O20}$ while in water and DMSO fallows as $LP_{O19} > LP_{O20} > LP_{O2} > LP_{O1}$ and $LP_{O1} > LP_{O19} > LP_{O20} > LP_{O2}$, respectively. In general, the electron transfer($LP_O→LP^*_{Ni}$) in the gas phase is more than that in water and DMSO leading to the lesser value of equilibrium constant in the gas phase than that in water and DMSO. Similarly, in the $[Ni(L_m)_2]$ complex, these interactions fallow as $LP_{O1} > LP_{O14} > LP_{O15} > LP_{O2}$, $LP_{O14} > LP_{O15} > LP_{O2} > LP_{O1}$ and $LP_{O14} > LP_{O15} > LP_{O1} > LP_{O2}$ in the gas, water and DMSO, respectively.

Ligand to Metal Charge Transfer

To obtain the individual atomic charges of the donor ligand atoms and metal ions in the complexes, the natural population analysis (NPA) was carried out in gas, water and DMSO phases at M062X/6-311++g(d,p) level of theory and the results are summarized in Table 6. Based on the results, the coordination of metal ion with L_f, L_d and L_m has induced delocalization of charges from the donor ligand atoms to the metal ions and from metal ions to the ligand atoms. As the table shows for the L_f ligand, the amount of net charge on donor ligand atoms O1(O29) and O2(O28) before complex formation in the gas phase is found to be -0.732, -0.603e, respectively. After the complex formation, it was noticed that the net charge on the O1(O29) and O2(O28) oxygen atoms are found to be increased by 0.086 and 0.097e for $[Ni(L_f)_2]$ complexes. Clearly, solvent increased the negative charge value for the O1(O29) and O2(O28) monomer donor atoms while this value has increased only by 0.040e after metal chelation process indicating that the solvent has a promoting effect on the chelation process. The trends observed for L_d ligand indicated that the negative charge value of O1(O19) and O2(O20) donor atoms in the monomer are -0.782 and -0.690e, respectively, while these values are decreased by 0.033 and 0.004e after complex formation in the gas phase. The net negative charge on the surfaces of donor atoms in L_d are more than that on the atoms in the L_f chelator. These values are increased

Table 6. The NPA Charges (e) for [Ni(L)$_2$] Complexes. Values within the Parentheses and Brackets Represent the Results Obtained at Water and DMSO Solvent Phases, Respectively)

Complex	Atom	Before complexation	After complexation
[Ni(L$_f$)$_2$]	O1	-0.732 [-0.814] {-0.813}	-0.818 [-0.843] {-0.843}
	O2	-0.603 [-0.664] {-0.664}	-0.680 [-0.704] {-0.704}
	O28	- [-] {-}	-0.818 [-0.843] {-0.843}
	O29	- [-] {-}	-0.680 [-0.704] {-0.704}
	M	2.000 [2.000] {2.000}	1.275 [1.345] {1.345}
[Ni(L$_d$)$_2$]	O1	-0.782 [-0.872] {-0.871}	-0.749 [-0.825] {-0.855}
	O2	-0.690 [-0.785] {-0.784}	-0.686 [-0.789] {-0.788}
	O19	- [-] {-}	-0.750 [-0.843] {-0.855}
	O20	- [-] {-}	-0.686 [-0.789] {-0.788}
	M	2.000 [2.000] {2.000}	1.040 [1.276] {1.307}
[Ni(L$_m$)$_2$]	O1	-0.789 [-0.871] {-0.870}	-0.780 [-0.815] {-0.851}
	O2	-0.656 [-0.723] {-0.722}	-0.686 [-0.751] {-0.727}
	O14	- [-] {-}	-0.780 [-0.839] {-0.851}
	O15	- [-] {-}	-0.686 [-0.732] {-0.727}
	M	2.000 [2.000] {2.000}	1.188 [1.303] {1.330}

similarly to L_f ligand in the presence of solvents however the negative net charge of donor atoms are decreased after complexation. Similar to L_d, in L_m chelator, the net charge of oxygen atoms showed more negative charge before complexation and the solvent like L_d has the same effect on the net negative charge of donor atoms. After the complex formation, it was noticed that the net charge on the O1(O15) and O2(O14) oxygen atoms in gas phase are found to be decreased by 0.009 and 0.056e, respectively. Similarly, the calculated net charges on Ni^{2+} ion for $[Ni(L)_2]$ complexes are found to be 1.275 for L_f, 1.040 for L_d, and 1.188e for L_m complexes for the gas phase. For $[Ni(L_f)_2]$, $[Ni(L_d)_2]$ and $[Ni(L_m)_2]$ complexes, 0.725, 0.960 and 0.812e amounts of positive charge are found to be neutralized in the gas phase calculations, respectively. In all the three $[Ni(L)_2]$ complexes in the solvent, the Ni^{2+} center retains more positive charge when it is chelated to the metal chelators. The results imply that the metal to ligand charge transfer interactions are more prominent for $[Ni(L_d)_2]$ interactions than those for $[Ni(L_f)_2]$ and $[Ni(L_m)_2]$ in the gas phase. Also, it could be concluded that the metal center in the solvent has a more positive charge than in gas phase. Based on the results, the inclusion of solvent (water and DMSO) leads to decrease in the amount of charge transfer between the metal ions and donor ligand atoms.

Topological Properties

The AIM-based analysis of electron density could provide valuable information on many physical and chemical properties of the molecular systems [43]. Topological analysis of the electron density was performed using AIM2000 program. In this regards, the following parameters are discussed: (a) electron density at bond critical point (BCP), ρBCP, (b) its Laplacian $\nabla^2\rho$, (c) ellipticity of the bond, (d) *ion/cov* parameter, and (e) the ratio of densities of potential and kinetic electron energies, V_{BCP} and G_{BCP} (V/G) [44-46].

Generally, the greater is the value of electron density at the given BCP, the stronger is the given bond [47]. Figure 4 represents the molecular graphs, electron density of the critical bonds point, their Laplacian and the ratio of densities of potential and kinetic electron energies (-V/G) in the studied complexes. It is expected that the stronger bonds are associated with higher electron density in the Ni-O bond

in all three complexes. The value of Ni-O bond ρ varies from 0.035 to 0.048 a.u for $[Ni(L_f)_2]$, 0.044 to 0.047 a.u for $[Ni(L_d)_2]$ and 0.033 to 0.053 a.u for $[Ni(L_m)_2]$ chelated complexes. It is observed that the inclusion of solvent slightly decreases the electron density at BCP for Ni-O coordination bonds which agreed with the structural parameters. The smallest value for $[Ni(L_f)_2]$ is observed for the Ni-O2(28) bond in the gas, water and DMSO and the most strength bond is associated with the Ni-O1(29) bond with $\rho = 0.048$ in the gas phase.

This shows that charge transfer interactions between the electronegative oxygen of chelator with metal ion is stronger rather than interactions between other oxygen atoms of L_f. Similarly, in the $[Ni(L_d)_2]$ complex, the highest value was observed for bond Ni-O1(19) with $\rho = 0.047$ in the water and the smallest value with $\rho = 0.036$ belongs to Ni-O1(29) in DMSO. The most strong bond in $[Ni(L_m)_2]$ complex belongs to the Ni-O1(15) bond in the gas phase. It is worth noting that the Ni-O bonds in the $[Ni(L_m)_2]$ have more ρ values than in others complexes. Comparison of the $[Ni(L)_2]$ complexes shows that the Ni-O coordination bonds have the slight variations in their electron density at BCP either in gas phase and in solvents.

The value of Laplacian of the electron density, $\nabla^2\rho$, may adopt both positive or negative value. Therefore, the closed shell interactions are characterized with positive values of $\nabla^2\rho$ which may belong to, *e.g.*, hydrogen bonds. A shared interaction (covalent bond) is characterized with $\rho > 0$ au and $\nabla^2\rho > 0$ at BCP [48]. In all three complexes, the Laplacian of the electron density, $\nabla^2\rho$, values at the bond critical points, BCPs, has a positive value, confirming the electronic charge is depleted in the interatomic region which is a characteristic of the closed-shell interactions in Ni-O bonds.

Another reliable tool in QTAIM analysis is the potential energy density to kinetic energy density ratio, -V/G, that may be applied to determine the nature of a chemical bond. Ionic interactions typically are determined by -V/G > 1 [49]. In all three complexes, the ionic nature of Ni-O bonds is obvious. The ionic nature of the gas phase of $[Ni(L)_2]$ complexes could be considered as $[Ni(L_m)_2] > [Ni(L_d)_2] > [Ni(L_f)_2]$. Ionic strength of Ni-O bonds has a slight decrease in the presence of solvents which could be considered as $[Ni(L_d)_2] > [Ni(L_m)_2] > [Ni(L_f)_2]$ and $[Ni(L_f)_2] > [Ni(L_d)_2] >$
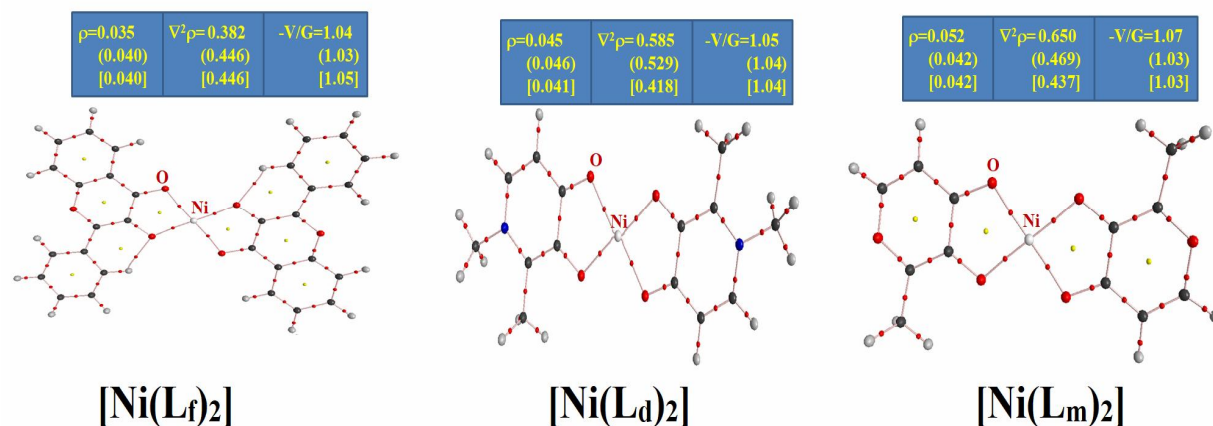
Fig. 4. Average values of selected QTAIM parameters of Ni-O bonds in the [Ni(L)$_2$] complexes: electron density at BCP, ρ, its Laplacian, $\nabla^2\rho$, and (-V/G) ratio. Values within the parentheses and brackets represent the results obtained at water and DMSO solvents, respectively.

Table 7. Average Values of the Selected QTAIM Parameters of M-O Bonds in the [Ni(L)$_2$] Complexes: $\lambda1$, $\lambda2$ and $\lambda3$, Bond Ellipticity, ε and *Ion/cov* Parameter. Values within the Parentheses and Brackets Represent the Results Obtained at Water and DMSO Solvent Phases, Respectively

Complex	Bond	$\lambda1$	$\lambda2$	$\lambda3$	ε	*Ion/cov*
[Ni(L$_f$)$_2$]	Ni-O	-0.072	-0.097	0.679	0.258	0.279
		(-0.111)	(-0.090)	(0.646)	(0.233)	(0.172)
		[-0.111]	[-0.090]	[0.646]	[0.233]	[0.172]
[Ni(L$_d$)$_2$]	Ni-O	-0.106	-0.094	0.672	0.127	0.158
		(-0.129)	(-0.108)	(0.772)	(0.117)	(0.167)
		[-0.110]	[-0.091]	[0.648]	[0.111]	[0.170]
[Ni(L$_m$)$_2$]	Ni-O	-0.159	-0.134	0.944	0.187	0.168
		(-0.110)	(-0.093)	(0.672)	(0.183)	(0.164)
		[-0.109]	[-0.089]	[0.634]	[0.225]	[0.172]

[Ni(L$_m$)$_2$] in water and DMSO, respectively.

The *ion/cov* parameter, defined as $|\lambda_1|/\lambda_3$ ratio and derived from the eigenvalues of the electron density Hessian, has been proposed as another measure of bond covalency [50]. Generally, the value of ion/cov parameter is <1 for closed shell interactions and >1 for shared interactions [51]. Table 7 represented eigenvalues of the electron density Hessian and the *ion/cov* values of the studied complexes. In all three complexes this value is in accordance to the closed shell interaction which is ionic in character. Table 7 represents the *ion/cov* values of the Ni-O bonds. The average values of Ni-O bond in the gas phase were calculated as 0.259, 0.158 and 0.168 for [Ni(L$_f$)$_2$], [Ni(L$_d$)$_2$] and [Ni(L$_m$)$_2$], respectively. The solvents have a

negative effect on the *ion/cov* parameters. This remains in a good agreement with the results of the other calculations reported above.

Another parameter derived from the Hessian of the electron density, the bond ellipticity, is small in all cases, indicating the predominance of sigma-type character of the bonds between the oxygen lone pairs and both central metal ions [52]. From Table 7, it could be concluded that the sigma- character of Ni-O bonds would be as follows: $[Ni(L_f)_2] > [Ni(L_m)_2] > [Ni(L_d)_2]$ in the gas, water and DMSO phases.

The NCI analysis can be used to determine the attractive and repulsive interactions based on electron density and the sign of the second derivative in perpendicular direction of the bond (λ2) [53]. To get a comprehensive understanding of the nature of interactions, NCI-RDG analysis was applied on the $[Ni(L)_2]$ complexes. This analysis, provide a clear description of the interactions in the real-space through a graphical visualization of the regions having a noncovalent nature [54]. The regions of NCI-RDG plots are classified as: H-bonding interactions (large negative value of sign $(\lambda_2)\rho$), Van der Waals interactions (spike very near to zero $(\lambda_2 \leq 0)$) and strong steric repulsion (large positive value of sign $(\lambda_2)\rho$, which are designed in the RDG isosurface with blue and red colors, respectively. In all cases, the isosurfaces were visualized with VMD 1.9.2 [55]. Figures 5(A, B, C) shows a 2D NCI plot of $[Ni(L_f)_2]$, $[Ni(L_d)_2]$ and $[Ni(L_m)_2]$. According to the positive character of λ_2 in Fig. 5, the main interactions during the chelation process are characterized as steric effects and Van der Waals attraction. To this content, in 2D NCI plots, the strength of steric interaction between the selected metal chelators and Ni^{2+} is in accordance to the $[Ni(L_f)_2] > [Ni(L_m)_2] > [Ni(L_d)_2]$ trend. In the NCI-RDG RDG-isosurface of the studied complexes we can conclude that the nature of the chelation interactions in $[Ni(L)_2]$ is a complete set of electrostatic interactions encompassing Van der Waals interactions (Figs. A', B', C'). Clearly, the results show that the H-bonding interactions are absent in all three complexes and has no effect on the chelation process of metal center and chelators.

DFT Reactivity Indices

HOMO-LUMO analysis was performed to evaluate the DFT reactivity indices. Based on this analysis, electronic chemical hardness, η, electronic chemical potential, μ, and global electrophilicity index, ω, were calculated [56]. The results are depicted in Table 8.

Based on the results, all HOMO-LUMO energy gaps are equal to 5.25, 5.91 and 6.10 eV for the $[Ni(L_f)_2]$, $[Ni(L_d)_2]$ and $[Ni(L_m)_2]$ in the gas phase, respectively. It was also found that the HOMO-LUMO energy gaps of the isolated chelators have the values about 4.17, 3.29 and 4.08 eV for HL_f, HL_d and HL_m, respectively, calculated at the same levels of theory at the gas phase, indicating that the isolated chelators have less stability with more chemical reactivity than their correspond complexes. Whereas, the interaction of metal ions with the chelators increases the HOMO-LUMO energy gap, resulting in the decreased chemical reactivity which further results in the stabilization of the kinetic stability with respect to the isolated chelators. The $[Ni(L_d)_2]$ complex has the lowest energy separation indicating the stronger chemical hardness, whereas the $[Ni(L_f)_2]$ complex shows the largest energy separation indicating a weaker chemical hardness. The energy gap value of $[Ni(L_m)_2]$ complexes has the intermediate range between the $[Ni(L_f)_2]$ and $[Ni(L_d)_2]$ complexes. The lower energy gap for $[Ni(L_d)_2]$ complex indicates that the interaction between ligand atoms and the metal ion are dominated by charge transfer interactions than electrostatic interactions. Furthermore, it is worthy to note that inclusion of the solvent effect leads to increase the HOMO-LUMO gap in the $[Ni(L_f)_2]$ complex which shows that the inclusion of solvents has a negative influence in the chelation process of $[Ni(L_f)_2]$. Increasing the η, in $[Ni(L_d)_2]$ due to inclusion of water solvent leads to destabilizing of chelated complex while an inverse effect was observed in the presence of DMSO. In $[Ni(L_m)_2]$, the presence of water causes to stabilizing the chelated complex while the DMSO solvent destabilized the chelated form due to decrease of HOMO-LUMO gap. The electrophilicity indices were calculated using the electronic chemical potential and electronic chemical hardness concepts. The global electrophility indexes of isolated chelators have lesser values than their chelated form. The gas phase ω values were found to be 1.69, 0.90 and 0.95 for $[Ni(L_f)_2]$, $[Ni(L_d)_2]$ and $[Ni(L_m)_2]$, respectively. The higher global electrophilicity index of $[Ni(L_f)_2]$ indicated that HLf
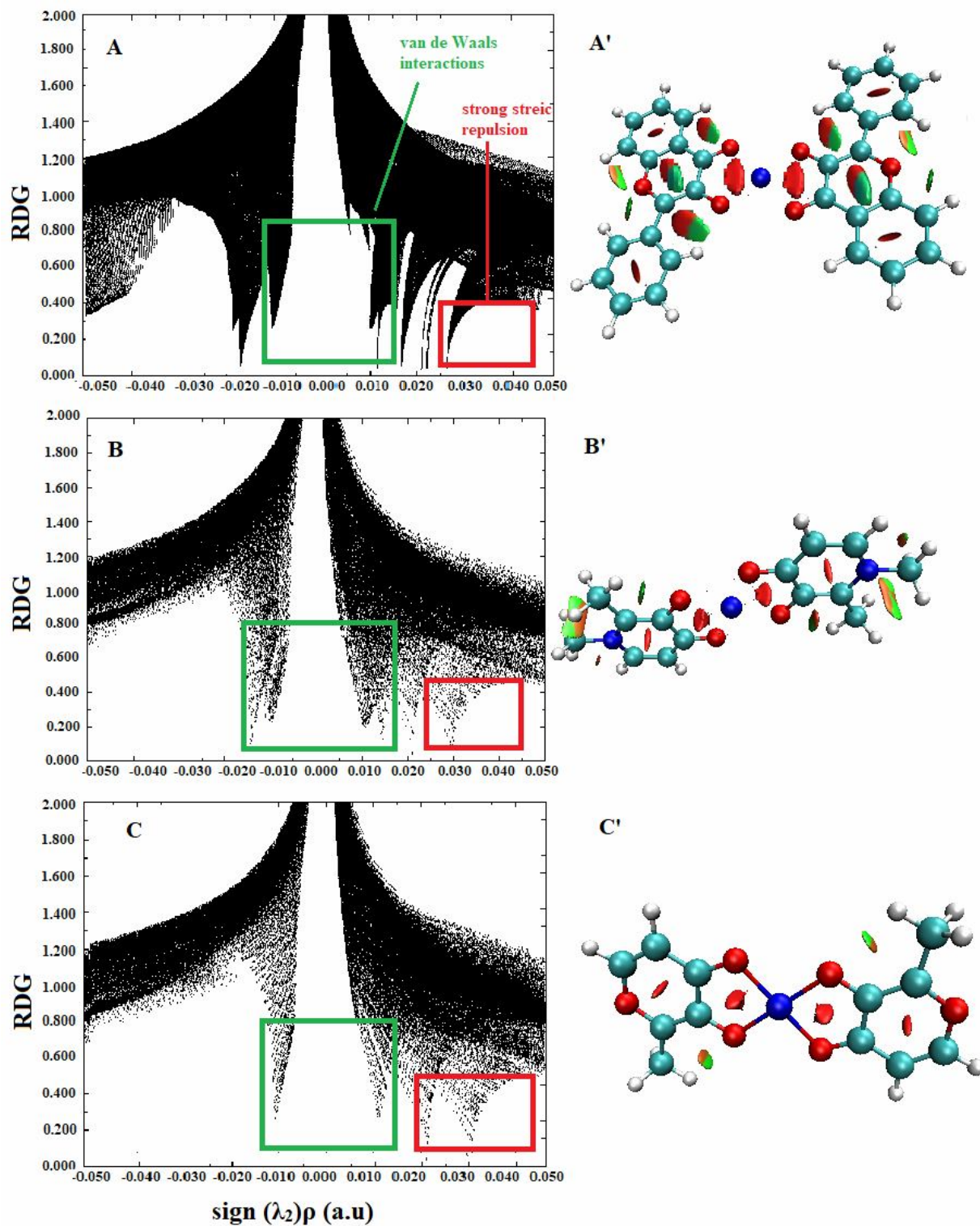
Fig. 5. Two-dimensional (2D) and 3D NCI plots of the (A,A') [Ni(L$_f$)$_2$] (B,B') [Ni(L$_d$)$_2$] (C,C') [Ni(L$_m$)$_2$] complexes.

Table 8. The HOMO and LUMO Energy and Energy Gap in the Gas, [Water] and {DMSO}

Complex	HOMO	LUMO	η	μ	Ω
	-6.85	-1.60	5.25	4.21	1.69
$[Ni(L_f)_2]$	[-7.05]	[-1.74]	[5.31]	[4.40]	[1.82]
	{-7.04}	{-1.73}	{5.31}	{4.40}	{1.82}
	-2.22	1.95	4.24	0.14	0.0023
HL_f	[-5.93]	[-0.99]	[4.94]	[3.46]	[1.21]
	{-5.97}	{-1.03}	{4.94}	{3.50}	{1.24}
	-6.22	-0.31	5.91	3.27	0.90
$[Ni(L_d)_2]$	[-6.84]	[-0.28]	[6.56]	[3.56]	[0.91]
	{-6.51}	{-0.71}	{5.80}	{3.61}	{1.12}
	-1.23	2.06	3.29	0.42	0.0268
HL_d	[-5.61]	[0.03]	[5.58]	[2.79]	[0.6975]
	{-5.56}	{0.05}	{5.51}	{2.77}	{0.6962}
	-6.95	-0.85	6.10	3.40	0.95
$[Ni(L_m)_2]$	[-7.01]	[-1.19]	[5.82]	[4.1]	[1.44]
	{-7.36}	{-0.74}	{6.62}	{4.05}	{1.24}
	-1.62	2.46	4.08	0.59	0.0427
HL_m	[-6.03]	[0.08]	[5.95]	[2.98]	[0.7463]
	{-5.99}	{0.10}	{5.89}	{2.96}	{0.7438}

has a lower tendency to make a chelated form with Ni^{2+} ion, whereas $[Ni(L_d)_2]$ and $[Ni(L_m)_2]$ have a similar tendency to make chelated complex. Inclusion of solvent has a negative effect on chelation process in all three complexes.
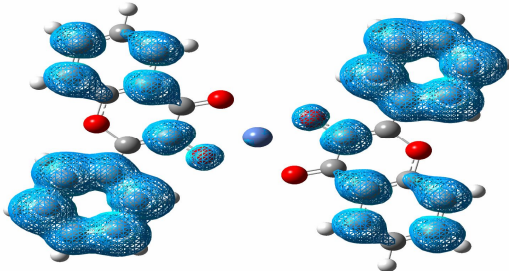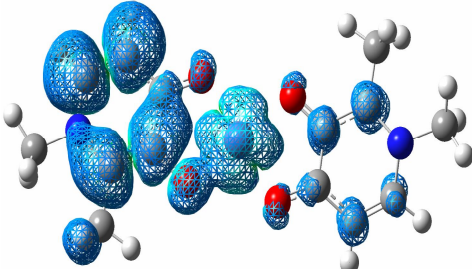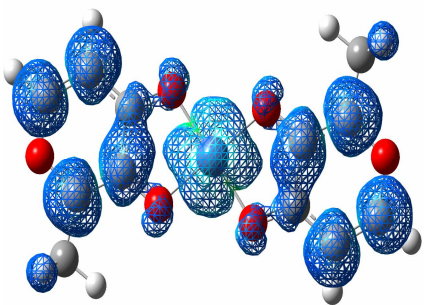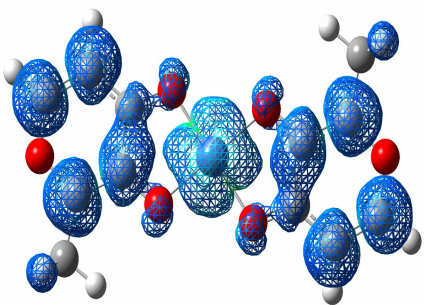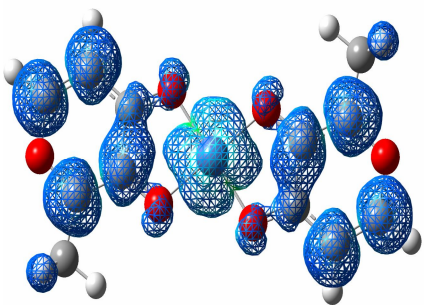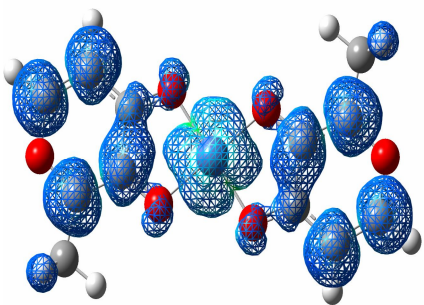
Spin Density Evaluation

In order to investigate the spin density distribution of the unpaired d-electrons of the studied Ni(II) complexes, the spin density values of the various atoms were calculated at the M062X/6 311++g(d,p) level of theory and the results are summarized in Table 9. The spin density distribution on Ni atom is according to $[Ni(L_m)_2] > [Ni(L_d)_2] > [Ni(L_f)_2]$ in the gas phase, while this trend has changed to $[Ni(L_f)_2] > [Ni(L_m)_2] > [Ni(L_d)_2]$ in both water and DMSO. Clearly, in

the presence of solvent, spin density distribution on the central atom has increased. Spin density on the coordinated oxygen atoms showed the highest value for $[Ni(L_d)_2]$ coordinated atoms, while the solvents have a negative impact on spin density distribution on the oxygen atoms in this complex. Similar trends were observed for the $[Ni(L_m)_2]$ and $[Ni(L_f)_2]$ complexes. According to the spin density values, there is a positive spin density distribution, which is related to the spin delocalization mechanism.

CONCLUSIONS

We have investigated the metal chelating properties of $[Ni(L_2)]$ chelates, where L represents the corresponding

Table 9. Spin Density Plots for Gas Phase State and Spin Density Values at the Coordinated Atomic Sites of [Ni(L)$_2$] Complexes. Values within the Parentheses and Brackets Represent the Results Obtained at Water and DMSO Solvent Phases, Respectively)

Complex	Atom	Spin density	
[Ni(L$_F$)$_2$]	Ni	1.76 (1.83) [1.83]	
	O1(28)	0.066 (0.054) [0.044]	
	O2(29)	0.036 (0.033) [0.033]	
[Ni(L$_D$)$_2$]	Ni	1.78 (1.80) [1.80]	
	O1(19)	0.069 (0.054) [0.038]	
	O2(20)	0.043 (0.038) [0.038]	
[Ni(L$_M$)$_2$]	Ni	1.77 (1.82) [1.82]	
	O1(14)	0.075 (0.056) [0.056]	
	O2(15)	0.041 (0.034) [0.034]	

metal chelators (L_f: 3-hydroxyflavone, L_d: deferepirone and L_m: maltol) at the M062X/6-311++g(d,p) level of theory in gas, water and DMSO phases, and the following results emerged from the detailed calculations. The optimized structures had a distorted tetrahedral coordination geometry. The equilibrium constant of complexes showed that the stability of the L-Ni complexes is as follows $[Ni(L_d)_2] > [Ni(L_m)_2] > [Ni(L_f)_2]$ both in the gas and solvent which verified the good chelation property of deferiprone as a known metal chelator. The LOL and ELF analyses revealed the electrostatic interactions between the metal chelators and the Ni^{2+} ion. The TD-DFT showed a single peak in the region between 272-362 nm. The highest value of wavelength was observed for $[Ni(L_f)_2]$ in the gas phase. The NBO analysis showed that there is an effective chemical bond between the chelators coordinated atoms and Ni ion due to high electron transfer to the antibonding Ni orbitals. Also, it was clear that Ni atom acts as an electron acceptor center. From the QTAIM analysis, electron density at bond critical point (BCP), ρBCP, its Laplacian, $\nabla^2\rho$, ellipticity of the bond, *ion/cov* parameter, and the ratio of densities of potential and kinetic electron energies, V_{BCP} and G_{BCP} (V/G), were calculated; the results confirmed a closed shell interaction between the oxygen donor atoms and Ni^{2+} ion. The NCI-RDG isosurface of the studied complexes showed a complete set of electrostatic interactions which encompass Van der Waals interactions. The spin density values showed a positive spin density distribution, due to the spin delocalization mechanism in the studied complexes. Consequently, the obtained results may be of a large applicative interest, since the selected metal chelators can act as a best chelating agents. Thus, the chelators are multipotent agents and can be used in chelation therapies for many neurodegenerative diseases such as Alzheimer's disease. Our study reveals that HL_f, HL_d and HL_m can form active chelates with the Ni^{2+} ion and they can be used as a chelating agent where the accumulation of Ni^{2+} ion is found to be dominant.

ACKNOWLEDGEMENTS

REFERENCES

[1] Asmaria, M.; Michalcováa, L.; Alhazmic, H. A.; Glatzb, Z.; ElDeeb, S., Investigation of deferiprone binding to different essential metal ions using microscale thermophoresis and electrospray ionization mass spectrometry, *Microchem. J.,* **2018**, *137*, 98-104, DOI: 10.1016/j.microc.2017.10.004.

[2] Sai Sathish, R.; Goutam Raju, A.; Nageswara Rao, G.; Janardhana, C., A fluorescent fluoride ion probe based on a self-organized ensemble of 5-hydroxyflavone-Al(III) complex, Spectrochim. *Acta A,* **2008**, *69*, 282-285, DOI: 10.1016/j.saa.2007.04.018.

[3] Eybl, V.; Kotyzova, D.; Kolek, M.; Koutensky, J.; Nielsen, P., The influence of deferiprone (L1) and deferoxamine on iron and essential element tissue level and parameters of oxidative status in dietary iron-loaded mice, *Toxicol. Lett.,* **2002**, *128*, 169-175, DOI: 10.1016/S0378-4274(01)00541-0.

[4] Gaeta, A.; Hider, R. C., The crucial role of metal ions in neurodegeneration: the basis for a promising therapeutic strategy, *Br. J. Pharmacol.,* **2005**, *146*, 1041-1059, DOI: 10.1038/sj.bjp.0706416.

[5] Bolognin, S.; Drago, D.; Messori, L.; Zatta, P., Chelation therapy for neurodegenerative diseases, *Med. Res. Rev.,* **2009**, *29*, 547-570, DOI: 10.1002/med.20148.

[6] Hossain, D.; Rana, U.; Chakraborty, C.; Li, J.; Nagano, R.; Minowa, T.; Higuchi, M., Effect of metal–metal distance in Ni(II)-based metallo-supramolecular polymers: DNA binding and cytotoxicity, *RSC Adv.,* **2017**, *7*, 38008- 38013, DOI: 10.1039/C7RA05644C.

[7] Jesu Jaya Sudan, R.; Lesitha Jeeva Kumari, J.; Sudandiradoss, C., Single cell adhesion assay using computer controlled micropipette, *PLoS ONE,* **2017**, *10*, 13-19, DOI: 10.1371/journal.pone.0111450.

[8] Birmanns, S.; Rusu, M.; Wriggers, W., Using Sculptor and Situs for simultaneous assembly of atomic components into low-resolution shapes, *J. Struct. Biol.,* **2011**, *173*, 428-35, DOI: 10.1016/j.jsb.2010.11.002 09153121682.

[9] Bork, P.; Koonin, E. V., Protein sequence motifs, *Curr. Opin. Struct. Biol.,* **1996**, *6*, 366-376, DOI: 10.1016/S0959-440X(96)80057-1.

[10] Denkhaus, E.; Salnikow, K., Nickel essentiality, toxicity, and carcinogenicity, *Crit. Rev. Oncol. Hematol.,* **2002**, *42*, 35-56, DOI: 10.1016/S1040-8428(01)00214-1.

[11] Kaviani, S.; Izadyar, M., The possibility of iron chelation therapy in the presence of different HPOs; a molecular approach to the non-covalent interactions and binding energies, *J. Mol. Stru.,* **2018**, *1166*, 448-455, DOI: 10.1016/j.molstruc.2018.04.065.

[12] Crisponi, G.; Remelli, M., Iron chelating agents for the treatment of iron overload, *Coord. Chem. Rev.,* **2008**, *252*, 1225-240, DOI: 10.1016/j.ccr.2007.12.014.

[13] Crichton, R. R.; Dexter, D. T., Metal based neurodegenerative diseases-From molecular mechanisms to therapeutic strategies, R. J. Ward, *Coord. Chem. Rev.,* **2008**, *252*, 1189-1199, DOI: 10.1016/j.ccr.2007.10.019.

[14] Salehi, S.; Izadyar, M., Saljooghi, A. S., Interactions of deferasirox as a chelating agent with Al and Ga cations: A theoretical study on the [M(DFX)$_2$]3-nanostructures, *Phys. Chem. Res.,* **2018**, *6*, 67-82, DOI: 10.22036/pcr.2017.94247.1404.

[15] Davila, Y. A.; Sancho, M. I.; Almandoz, M. C.; Blanco, S. E., Structural and spectroscopic study of Al(III)-3-hydroxyflavone complex: Determination of the stability constants in water-methanol mixtures, *Spectrochimica Acta Part A: Mol. Biomo. Spect.,* **2012**, *95*, 1-7, DOI: 10.1016/j.saa.2012.04.034.

[16] Aherne, S. A.; O'Brien, N. M., Dietary flavonols: Chemistry, food content, and metabolism, nutrition, **2002**, 75-81, DOI: 10.1016/S0899-9007(01)00695-5.

[17] Siatka, T.; Kašparová, M., Seasonal variation in total phenolic and flavonoid contents and DPPH scavenging activity of bellis perennis L. flowers, *Molecules,* **2010**, *15*, 9450–9461, DOI: 10.3390/molecules15129450.

[18] Diamond, G. L.; Morrow, P. E.; Panner, B. J.; Gelein, R. M.; Baggs, R. B., Reversible uranyl fluoride nephrotoxicity in the long evans rat, *Fundam. Appl. Toxicol.,* **1989**, *13*, 65-78, DOI: 10.1016/0272-

0590(89)90307-2.

[19] Habgood, M. D.; Liu, Z. D.; Dehkordi, L. S.; Khodr, H. H.; Abbott, J.; Hider, R. C., Investigation into the correlation between the structure of hydroxypyridinones and blood-brain barrier permeability, *Biochem. Pharmacol.,* **1999**, *57*, 1305-1310, DOI: 10.1016/S0006-2952(99)00031-3.

[20] Fatemi, S. J.; Nejad, F. K.; Zandevakili, T.; Balooch, F. D.; Chelation of cobalt by combining deferasirox, deferiprone and desferrioxamine in rats, *Toxin Rev.,* **2014**, *33*, 146-150, DOI: 10.3109/15569543.2014.911749.

[21] Zhu, C. F.; Qiu, D. H.; Kong, X. L.; Hider, R. C.; Zhou, T., Synthesis and *in vitro* antimicrobial evaluation of a high-affinity iron chelator in combination with chloramphenicol, *J. Pharm. Pharmacol.,* **2013**, *65*, 512-520, DOI: 10.1111/jphp.12013.

[22] Fryzuk, M. D.; Jonker, M. J.; Rettig, S. J., Ruthenium maltolato complexes, *Chem. Comm.,* **1997**, *1997*, 377-378, DOI: 10.1039/a606961d.

[23] Kaviani, S.; Izadyar, M.; Housaindokht, M. R., Solvent and spin state effects on molecular structure, IR spectra, binding energies and quantum chemical reactivity indices of deferiprone-ferric complex: DFT study, *Polyhedron,* **2016**, *117*, 623-627, DOI: 10.1016/j.poly.2016.06.041.

[24] Kolarik, Z., Complexation and separation of lanthanides(III) and actinides(III) by heterocyclic N-donors in solutions, *Chem. Rev.,* **2008**, *108*, 4208, DOI: 10.1021/cr078003i.

[25] Cancès, E.; Mennucci, B.; Tomasi, J., A new integral equation formalism for the polarizable continuum model: Theoretical background and applications to isotropic and anisotropic dielectrics, *J. Chem. Phys,* **1997**, *107*, 3032-3041, DOI: 10.1063/1.474659.

[26] Csaba, G.; Birzele, F.; Zimmer, R., Systematic comparison of SCOP and CATH: a new gold standard for protein structure analysis, *BMC Struct. Biol.,* **2009**, *9*, 23-35, DOI: 10.1186/1472-6807-9-23.

[27] Loza-Rosas, S. A.; Vazquez-Salgado, A. M.; Rivero, K. I.; Negron, L. J., Expanding the therapeutic potential of the iron chelator deferasirox in the development of aqueous stable Ti(IV) anticancer

complexes, *Inorg. Chem.,* **2017**, *56*, 7788-7802, DOI: 10.1021/acs.inorgchem.7b00542.

[28] Salehi, S.; Saljooghi, A. S.; Shiri, A., Synthesis, characterization and *in vitro* anticancer evaluations of two novel derivatives of deferasirox iron chelator, *Eur. J. Pharm.,* **2016**, *781*, 209 -217, DOI: 10.1016/ j.ejphar.2016.04.026.

[29] Frisch, M. J.; Trucks, G. W.; Schlegel, H. B.; Robb, M. A.; Cheeseman, J. R.; Scalmani, G.; Scuseria, G. E.; Barone, V.; Mennucci, B.; Petersson, G. A., Gaussian 09, Revision A02, Gaussian Inc, Wallingford, CT, 2009.

[30] Barone, V.; Cossi, M., Quantum calculation of molecular energies and energy gradients in solution by a conductor solvent model, *J. Phys. Chem. A,* **1998**, *102*, 1995-2001, DOI: 10.1021/jp9716997.

[31] Hernandez, M. G.; Beste, A.; Frenking, G.; Illas, F., Charge decomposition analysis of the chemisorption bond, *Chem. Phys. Lett.,* **2000**, *320*, 222-228, DOI: 10.1016/S0009-2614(00)00160-3.

[32] Bader, R. F. W., A quantum theory of molecular structure and its applications, *Chem. Rev.,* **1991**, *91*, 893-928, DOI: 10.1021/cr00005a013.

[33] Lu, T.; Chen, F., Monomeric adenine decay dynamics influenced by the DNA environment, *J. Comput. Chem.,* **2012**, *33*, 580-592, DOI: 10.1002/jcc.22952.

[34] Chen, Z.; Wang, W.; Zhu, C.; Wang, L.; Fang, X.; Qiu, Y., Probing chemical bonding and optoelectronic properties of square-planar aluminum, gallium, and nickel complexes, *Comput. Theor. Chem.,* **2016**, *1090*, 129-133, DOI: 10.1016/j.comptc.2016.06.016.

[35] Boys, S. F.; Bernardi, F., Molecular physics: An international journal at the interface between chemistry and physics, *Mol. Phys.,* **1970**, *19*, 553-566, DOI: 10.1080/00268977000101561.

[36] Shankar, R.; Kolandaivel, P.; Senthil Kumar, L., Synthesis and characterization of di-/triorgano stannates bearing tin-sulfonate bonds, *Inorganica Chim. Acta.,* **2012**, *387*, 125-136, DOI: 10.1016/ j.ica.2012.02.040.

[37] Pitchumani, C.; Mary, V.; Shankar, R.; Vijayakumar, S.; Kolandaivel, P., Interaction studies of human prion protein (HuPrP109-111: methionine-lysine-histidine) tripeptide model with transition metal cations, *J. Mol.*

Graph.Model., **2016**, *69*, 111-126, DOI: 10.1016/ j.jmgm.2016.08.012.

[38] Yang, L.; Powell, D. R.; Houser, R. P., Structural variation in copper(I) complexes with pyridylmethylamide ligands: structural analysis with a new four-coordinate geometry index, τ4, *Dalton Trans.,* **2007**, *9*, 955-964, DOI: 10.1039/B617136B.

[39] Nkungli, N. K.; Ghogomu, J. N., Theoretical analysis of the binding of iron(III) protoporphyrin IX to 4-methoxyacetophenone thiosemicarbazone *via* DFT-D3, MEP, QTAIM, NCI, ELF and LOL studies, *J. Mol. Model.,* **2017**, *23*, 200-220, DOI: 10.1007/ s00894-017-3370-4.

[40] Politzer, P.; Murray, J. S., The fundamental nature and role of the electrostatic potential in atoms and molecules, *Theor. Chem. Accounts,* **2002**, *108*, 134-142, DOI: 10.1007/s00214-002-0363-9.

[41] Khavani, M.; Izadyar, M.; Housaindokht, M. R., Modeling of the functionalized gold nanoparticles aggregation in the presence of dopamine, A joint MD/QM study, *J. Phys. Chem. C,* **2018**, *122*, 26130-26141, DOI: 10.1021/acs.jpcc.8b06600.

[42] Cossi, M.; Barone, V.; Cammi, R., *Ab initio* study of solvated molecules: a new implementation of the polarizable continuum model, Tomasi, J., *J. Phys. Lett.,* **1996**, *255*, 327-335, DOI: 10.1016/0009-2614(96)00349-1.

[43] Strzelczyk, W.; Sobieszczyk, P.; Palusiak, M., Bonding in β-diketiminate boron and its analogues, *Struct. Chem.,* **2009**, *20*, 919-923, DOI: 10.1007/ s11224-009-9492-2.

[44] Krygowski, T. M.; Palusiak, M.; Płonka, A.; Zachara-Horeglad, J. E., Relationship between substituent effect and aromaticity-Part III: naphthalene as a transmitting moiety for substituent effect, *J. Phys. Org. Chem.,* **2007**, *20*, 297, DOI: 10.1002/poc.1127.

[45] Bader, R., Atoms in Molecules: A Quantum Theory: Oxford Univ. Press.: Oxford, 1990.

[46] Vidal, I.; Melchor, S.; Alkorta, I.; Elguero, J.; Sundberg, M. R.; Dobado, J. A., On the existence of r-agostic bonds: Bonding analyses of titanium alkyl complexes, *Organometallics,* **2006**, *25*, 5638, DOI: 10.1021/om0608197.

[47] Bader, R. F. W.; Matta, C. F.; Corte´s-Guzman, F.,

Where to draw the line in defining a molecular structure, *Organometallics,* **2004**, *23*, 6253, DOI: 10.1021/om049450g.

[48] Dutta, A., Hydrothermal growth of ZnO nanostructures, *Rev. Adv. Mater. Sci.,* **2014**, *39*, 25-33, DOI: 10.1088/1468-6996/10/1/013001

[49] Mitrasinovic, P. M., Acrylonitrile (AN)-Cu9(100) interfaces: Electron distribution and nature of bonded interactions, *Can. J. Chem.,* **2003**, *81*, 542, DOI: 10.1139/v03-043.

[50] Sola, M.; Mestres, J.; Carbo, R.; Duran, M., A comparative analysis by means of quantum molecular similarity measures of density distributions derived from conventional *ab initio* and density functional methods, *J. Chem. Phys.,* **1996**, *104*, 636, DOI: 10.1063/1.470859.

[51] Palusiak, M.; Krygowski, T. M., Application of AIM parameters at ring critical pPoints for estimation of p-electron delocalization in six-membered aromatic and quasi-aromatic rings, *Chem. Eur. J.,* **2007**, *13*, 7996, DOI: 10.1002/chem.200700250.

[52] Respondek, T.; Garner, R. N.; Herroon, M. K.; Podgorski, I.; Turro, C.; Kodanko, J. J., Light Activation of a cysteine protease inhibitor: Caging of a peptidomimetic nitrile with RuII(bpy)2, *J. Am. Chem. Soc.,* **2011**, *133*, 17164, DOI: 10.1021/ja208084s.

[53] Chaudret, R.; De Courcy, B.; Contreras-Garcia, J.; Gloaguen, E.; Zehnacker-Rentien, A.; Mons, M.; Piquemal, J. P., Unraveling non-covalent interactions within flexible biomolecules: from electron density topology to gas phase spectroscopy, *Phys. Chem. Chem. Phys.,* **2014**, *16*, 9876-9891, DOI: 10.1039/c3cp52774c.

[54] González, J.; Baňos, I.; León, I.; Contreras-Garcia, J.; Cocinero, E. J.; Fernádez, J. A.; Millán, J., Unravelling protein-DNA interactions at molecular level: A DFT and NCI study, *J. Chem. Theory Comput.,* **2016**, *12*, 523-534, DOI: 10.1021/acs.jctc.5b00330.

[55] Contreras-García, J.; Boto, R. A.; Izquierdo-Ruiz, F.; Reva, I.; Woller, T.; Alonso, M., A benchmark for the non-covalent interaction (NCI) index or… is it really all in the geometry?, *Theor. Chem. Accounts,* **2016**, *135*, 242, DOI: 10.1007/s00214-016-1977-7.

[56] Mehranfar, A.; Izadyar, M., Theoretical evaluation of symmetrical α,α′,δ,δ′-tetramethyl cucurbit[6]uril for haloalkane 1-(3-chlorophenyl)-4-(3-chloropropyl)-piperazinium and chloroform encapsulation, *J. Inclusion Phenomena and Macrocyclic Chem.,* **2018**, DOI: 10.1007/s10847-018-0820-2.